

Gamma-Ray Burst Intensity Distributions

David L. Band¹, Jay P. Norris and Jerry T. Bonnell

GLAST SSC, Code 661, NASA/Goddard Space Flight Center, Greenbelt, MD 20771

`dband@lheapop.gsfc.nasa.gov`

ABSTRACT

We use the lag-luminosity relation to calculate self-consistently the redshifts, apparent peak bolometric luminosities L_B , and isotropic energies E_{iso} for a large sample of BATSE bursts. We consider two different forms of the lag-luminosity relation; for both forms the median redshift for our burst database is 1.6. We model the resulting sample of burst energies with power law and Gaussian distributions, both of which are reasonable models. The power law model has an index of $\alpha = 1.76 \pm 0.05$ (95% confidence) as opposed to the index of $\alpha = 2$ predicted by the simple universal jet profile model; however, reasonable refinements to this model permit much greater flexibility in reconciling predicted and observed energy distributions.

Subject headings: gamma-rays: bursts

1. Introduction

The major breakthroughs in the study of gamma-ray bursts of the past six years—most if not all bursts are cosmological, bursts are *not* standard candles, the fireballs are beamed, many bursts are associated with supernovae—resulted from the intensive study of a relatively small number of bursts without regard for whether these bursts formed a well defined statistical sample. However, realizing that for any one burst we are only sampling an anisotropic radiation pattern from one direction, we now have to study distributions of burst properties to reconstruct what bursts look like from all directions. Well-defined burst samples are required to derive these distributions.

¹Joint Center for Astrophysics, Physics Department, University of Maryland Baltimore County, 1000 Hilltop Circle, Baltimore, MD 21250

Unfortunately, we do not yet have a large sample of bursts with redshifts, which in most cases are required for calculating the intrinsic burst properties. The two dozen or so bursts with redshifts were detected by various detectors with different detection thresholds and energy sensitivities, and the follow-ups that resulted in the redshifts depended on the vagaries of weather and telescope availability. BATSE provided a large burst sample with well-understood thresholds, but without direct redshift determinations for most of these bursts. However, redshifts can be determined indirectly from the lag-luminosity or variability-luminosity relations. Here we calculate self-consistently the redshifts for a large subset of the BATSE bursts using the lag-luminosity relation. To accommodate the problematic burst GRB980425, which is significantly underluminous if the lag-luminosity relation is a single power law, Salmonson (2001) and Norris (2002) proposed that the relation should be a broken power law. This reduces the luminosity of many long-lag bursts, moving this population closer to the observer.

We use the resulting redshifts to calculate both the peak bolometric luminosity L_B and the isotropic energy E_{iso} ; both quantities assume that the burst radiates isotropically. We consider the isotropic energy E_{iso} to be more fundamental, and therefore model the energy distribution.

The energy distribution can discriminate between the two proposed models for the structure of the jets. The uniform jet model (Frail et al. 2001; Bloom, Frail, & Kulkarni 2003) assumes that all jets have a constant surface energy density ϵ (energy per solid angle) but differing opening angles θ_o . The model makes no predictions for the energy distribution. In the universal jet profile model (Rossi, Lazzatti, & Rees 2002; Zhang & Meszaros 2002) all jets have the same surface energy density ϵ as a function of off-axis angle θ , and thus the observed differences in L_B or E_{iso} results from our angle θ_v relative to the jet axis. This model predicts that if the surface energy density ϵ is a power law with index k , $\epsilon \propto \theta^k$, then the energy distribution will be a power law with index $\alpha = 1 - 2/k$, where $N(E_{\text{iso}}) \propto E_{\text{iso}}^{-\alpha}$; hence $\alpha = 2$ for $k = -2$. A Gaussian profile results in $\alpha = 1$. Numerical modelling of hypernovae (Zhang, Woosley, & MacFadyen 2003) show that the surface energy density of the outflows should vary with off-axis angle, but do not predict the profile. Thus the profiles are empirical models to fit the data.

The simple universal jet profile model can be falsified by the observed energy distribution but the uniform jet model cannot. However, physically plausible refinements, such as allowing the parameters of the jet profile to vary somewhat from burst to burst—the jet profile is now only quasi-universal—results in much greater flexibility in reconciling predicted and observed energy distributions (Lloyd-Ronning et al. 2003). Nonetheless, we compare our calculated energy distributions to the predictions.

In these calculations we use a cosmology with $H_0 = 70 \text{ km s}^{-1} \text{ Mpc}^{-1}$, $\Omega_m = 0.3$ and $\Omega_\Lambda = 0.7$. We use the notation $p(a | b)$ to mean the probability of a given b .

In §2 we present the methodology used in this study: calculating the burst redshifts (§2.1); fitting the intensity distribution (§2.2); and using the cumulative probability to test the quality of the fit (§2.3). The implementation of this methodology is discussed in §3 and the results are provided by §4. Finally, our conclusions are in §5.

2. Methodology

2.1. Calculating Redshifts

In the absence of a large number of measured spectroscopic redshifts, we use the lag-luminosity relation (Norris et al. 2000) to calculate peak luminosities L_B , and subsequently redshifts, for a large burst sample. Assume that for a set of bursts we have measured the lag between the lightcurve in two energy bands τ_0 (s), the peak photon flux P ($\text{ph s}^{-1} \text{ cm}^{-2}$) in the energy band E_1 – E_2 , and the spectral fit for the time period over which P is measured. The spectral fit is characterized by the parameters α , β and E_p of the “Band” model (Band et al. 1993). The instrument team is assumed to have converted the observed peak count rate into the peak photon flux using the fitted spectral model and the response function.

The lag τ_B in the burst’s frame and the observed lag τ_0 , both between the same energy bands in their respective frames, are related by time dilation (which increases the lag) and spectral redshifting (which shifts the smaller lag at high energy into the observed band). The first effect is simple and universal—a factor of $(1 + z)^{-1}$. The second depends on the burst’s spectral evolution, and may vary from burst to burst. Thus

$$\tau_B = \tau_0 g(z) \quad . \quad (1)$$

We will assume that $g(z)$ is universal, and as an ansatz we assume $g(z) = (1 + z)^{c_\tau}$. Time dilation contributes -1 to c_τ , while the redshifting of temporal structure with a smaller lag from higher energy contributes a positive constant (e.g., $\sim 1/3$; Fenimore et al. 1995 found ~ 0.4).

Empirically the lag has been related to the apparent bolometric peak luminosity L_B (erg s^{-1} ; Norris et al. 2000)

$$L_B = Q(\tau_B) \quad . \quad (2)$$

The observed peak bolometric energy flux F_B is related to the bolometric peak lumi-

luminosity L_B through the redshift, and an assumed cosmology:

$$F_B = L_B/[4\pi D_L^2] \quad , \quad (3)$$

where D_L is the luminosity distance. Note that L_B is the “isotropic” peak luminosity, the peak luminosity if the observed flux were beamed in all directions. If the flux is actually beamed into a solid angle $\Delta\Omega$, then the actual peak luminosity is only $\Delta\Omega/4\pi$ of L_B . We define

$$\langle E \rangle = F_B/P \quad (4)$$

$$\text{where } P = \int_{E_1}^{E_2} N(E)dE \quad (5)$$

$$\text{and } F_B = \int_0^\infty EN(E)dE \quad ; \quad (6)$$

$N(E)$ is the photon spectrum.

The implicit equation for redshift,

$$P = \frac{Q(\tau_0 g(z))}{4\pi D_L^2 \langle E \rangle} \quad , \quad (7)$$

must be solved for each burst. The functional form of the lag-luminosity relation Q can be calibrated from the small set of bursts for which z is known (see below). We have an ansatz for $g(z)$ with one unknown constant c_τ . This constant can be calculated using the dependence of τ on energy bands (Fenimore et al. 1995). Alternatively c_τ can be fit simultaneously with the determination of Q .

For this large database we then have L_B , z , τ_0 , P and the spectral parameters for the peak of the lightcurve. This database can be used to study the distribution of intensity measures such as the total burst energy and the peak luminosity.

2.2. The Intensity Distribution

We use a Bayesian analysis to investigate intensity distributions. In this study we consider the total isotropic energy E_{iso} as the relevant intensity measure; the isotropic energy is the energy emitted if the observed flux were radiated isotropically and not beamed towards us. Note that the same formulae apply substituting L_B for E_{iso} .

Assume our burst database provides the isotropic energy E_{iso} , the peak flux P and the redshift z for each burst (Band 2001). The threshold peak flux P_{min} is assumed to be known,

from which the threshold isotropic energy $E_{\text{iso,min}}$ for each burst can be calculated: to first order $E_{\text{iso,min}} = E_{\text{iso}} P_{\text{min}}/P$. The energy distribution function is the normalized probability distribution $p(E_{\text{iso}} | \vec{a}_j, M_j, z, I)$ where \vec{a}_j is the set of parameters that characterize the j th model distribution function represented by M_j , and I specifies general assumptions about the distribution function. For generality the energy distribution function has been given a redshift dependence. However, the observed E_{iso} are not drawn from $p(L_B | \vec{a}_j, M_j, z, I)$ but from

$$p(E_{\text{iso}} | E_{\text{iso,min}}, \vec{a}_j, M_j, z, I) = \frac{p(E_{\text{iso}} | \vec{a}_j, M_j, z, I)\theta(E_{\text{iso}} - E_{\text{iso,min}})}{\int_{E_{\text{iso,min}}}^{\infty} dE_{\text{iso}} p(E_{\text{iso}} | \vec{a}_j, M_j, z, I)} \quad (8)$$

where $\theta(x)$ is the Heaviside function (1 for positive x and 0 for negative x); E_{iso} is drawn from the observable part of the luminosity function. We now form the likelihood

$$\Lambda_j = \prod_{i=1}^N p(E_{\text{iso},i} | E_{\text{iso,min},i}, \vec{a}_j, M_j, z_i, I) \quad (9)$$

where the i th burst has isotropic energy $E_{\text{iso},i}$, threshold isotropic energy $E_{\text{iso,min},i}$ and redshift z_i .

In the “frequentist” framework best-fit parameters are typically found by maximizing Λ_j . The Bayesian analysis is based on $p(\vec{a}_j | D, M_j, I)$, the posterior probability for the parameters; here D is the set of observed peak bolometric luminosities and their thresholds. Note that $\Lambda_j = p(D | \vec{a}_j, M_j, I)$. Thus an estimate of the parameters is

$$\begin{aligned} \langle \vec{a}_j \rangle &= \int d\vec{a}_j \vec{a}_j p(\vec{a}_j | D, M_j, I) = \frac{\int d\vec{a}_j \vec{a}_j p(D | \vec{a}_j, M_j, I)p(\vec{a}_j | M_j, I)}{\int d\vec{a}_j p(D | \vec{a}_j, M_j, I)p(\vec{a}_j | M_j, I)} \\ &= \frac{\int d\vec{a}_j \vec{a}_j \prod_{i=1}^N p(E_{\text{iso},i} | E_{\text{iso,min},i}, \vec{a}_j, M_j, z_i, I)p(\vec{a}_j | M_j, I)}{\int d\vec{a}_j \prod_{i=1}^N p(E_{\text{iso},i} | E_{\text{iso,min},i}, \vec{a}_j, M_j, z_i, I)p(\vec{a}_j | M_j, I)} \end{aligned} \quad (10)$$

where $p(\vec{a}_j | M_j, I)$ is the prior for the parameters \vec{a}_j . If $\Xi_j = p(D | \vec{a}_j, M_j, I)p(\vec{a}_j | M_j, I)$ is sharply peaked, then the expectation value of the parameters occurs at the peak of Ξ_j . Note that Ξ_j is the likelihood in eq. 9 times the priors for the parameters, and is proportional to the posterior probability $p(\vec{a}_j | D, M_j, I)$. The posterior probability is also used to determine the acceptable parameter range, which is often more meaningful than the “best” parameters values.

2.3. The Cumulative Probability

The Bayesian approach does not provide a goodness-of-fit statistic. However a frequentist statistic can be derived. For each burst the cumulative probability is

$$P(E_{\text{iso},i} | E_{\text{iso},\text{min},i}, \vec{a}_j, z_i, M_j, I) = \int_{E_{\text{iso},i}}^{\infty} p(E_{\text{iso}} | E_{\text{iso},\text{min},i}, \vec{a}_j, z_i, M_j, I) dE_{\text{iso}} \quad . \quad (11)$$

If the assumed energy distribution function is an acceptable characterization of the observations (which would be the case if the model M_j is correct) and all the assumptions are valid (e.g., the cosmological model is correct), then the cumulative probabilities $P(E_{\text{iso},i})$ should be uniformly distributed between 0 and 1, and have an average value of $\langle P(E_{\text{iso},i}) \rangle = 1/2 \pm (12N)^{-1/2}$ for N bursts in the sample.

3. Implementation

3.1. Datasets

Our data are all derived from various BATSE burst databases. We start with a database for 1438 bursts that includes the lags and their uncertainties, the peak flux P on the 256 ms timescale, the burst duration T_{90} , and hardness ratios among the 4 BATSE energy channels (30–50, 50–100, 100–300, and 300–2000 keV). Of these 1438 bursts, 1218 have positive lags.

To calculate the average energy $\langle E \rangle$ (see eq. 4) we use the parameters of “Band” spectrum fits by Mallozzi et al. (1998) to the 16 channel BATSE “CONT” count spectra accumulated over the peak flux time interval (usually 2.048 s) for the 580 bursts in our database that are also in the Mallozzi et al. database. For the 858 bursts that are not in the Mallozzi et al. database we assume the average low and high energy spectral indices of $\alpha = -0.8$ and $\beta = -2.3$ found by Preece et al. (2000). Because E_p , the energy of the peak of the $EN(E) \propto \nu f_\nu$ curve, and HR_{32} , the 100–300 keV to 50–100 keV hardness ratio, are strongly correlated, we use the empirical relation $E_p = 240 \text{ HR}_{32}^2$ keV (for $\text{HR}_{32} \leq 2.25$) for the bursts without spectral fits. Figure 1 shows the resulting scatter plot for E_p vs. HR_{32} .

3.2. The Lag-Luminosity Relation

Based on less than a dozen bursts, Norris et al. (2000) found that $L_B \propto \tau_B^{-1.15}$. However, this single component relationship predicts a much greater L_B than observed for GRB980425, the burst that appears to coincide with the supernova SN1998bw. By introducing a break

in the lag-luminosity relation Salmonson (2001) and Norris (2002) were able to include GRB980425. The resulting lag-luminosity relation is:

$$L_{51} = 2.18(\tau/0.35 \text{ s})^{c_L}, \quad c_L = -1.15 \text{ for } \tau \leq 0.35 \text{ s}, \quad -4.7 \text{ for } \tau > 0.35 \text{ s}. \quad (12)$$

where $L_{51} = L_B/10^{51} \text{ erg s}^{-1}$. In our calculations we use both the single (i.e., $c_L = -1.15$ for all τ) and two component lag-luminosity relations.

4. Results

4.1. Lag-Luminosity Relation and Redshift

We first investigate the lag-luminosity relation. Salmonson (2001) and Norris (2002) introduced a break in the simple power law relation to include the long lag, very low luminosity GRB980425. As a result of this break other long lag bursts in the BATSE database are assigned low luminosities, and consequently small distances; Norris suggests that there may be a population of nearby low luminosity bursts. Figure 2 demonstrates this: the solid line is the cumulative distribution of burst redshifts assuming a single power law lag-luminosity relation, while the dashed line shows the distribution for the broken power law. Introducing a break in the power law shifts the low redshift bursts closer. Note this break is included only to include GRB980425 in the lag-luminosity relation; if GRB980425 was not associated with SN1998bw or if GRB980425 was anomalous, then this break is unnecessary and unsupported by other data.

Figure 2 also shows that there are few bursts with $z > 10$. These bursts may indeed be at high redshift; finding such high redshift bursts is one of the goals of the Swift mission. However, on theoretical grounds bursts with $z > 17$ are not expected. Given the dispersion in the lag-luminosity relation, it is not surprising that some bursts are assigned redshifts as high as $z = 65$; large redshifts result from high luminosities for bursts with very small lags, which are particularly difficult to measure accurately. Thus the lag-luminosity relation does not give unphysical results at the high luminosity end. Norris (2002) placed an upper limit on the luminosity when he found a large number of very high redshift bursts.

We use the simple single power law lag-luminosity relation without any cutoffs or limits in the following analysis.

For our database the median redshift is $z_m = 1.58$. As can be seen from Figure 1, this redshift is greater than the redshift range where the form of the lag-luminosity relation makes a difference.

4.2. The E_{iso} Distribution

We focus on the distribution functions of the bolometric energy. To perform quantitative estimates of distributions as a function of redshift (e.g., of the burst rate) the threshold for the database must be known, and therefore studies have often focused on the peak luminosity L_B ; L_B is more closely related to the peak flux P , which has a relatively sharp instrumental threshold P_{min} . However, to study distributions of intrinsic burst quantities the threshold for that quantity for each observed burst will suffice. Thus our database is sufficient to study both the isotropic energy E_{iso} and the peak luminosity L_B distributions.

Figure 4 shows the scatter plot of the isotropic energy E_{iso} . The region just above the threshold is underpopulated, suggesting that the thresholds are underestimated. Therefore, we raise the threshold to $P_{\text{min}} = 0.5 \text{ ph cm}^{-2} \text{ s}^{-1}$. This raises the median redshift from 1.58 to 1.62.

4.2.1. Power Law E_{iso} Distribution

Universal jet structure models predict a power law energy distribution function with an index of $\alpha = 2$ ($p(E_{\text{iso}}) \propto E_{\text{iso}}^{-\alpha}$); for a finite number of bursts the distribution must have a low energy cutoff E_2 . We therefore fit our burst sample with this distribution function. Figure 5 shows the resulting likelihood surface which peaks at $\alpha = 1.76$ and $\log(E_2) = 50.2$. This value of E_2 is the smallest value of E_{iso} in our sample; burst samples that extend to fainter bursts will probably have smaller observed values of E_{iso} , and consequently E_2 is most likely smaller. The contour plot indicates that the determination of α is independent of the value of E_2 . The 95% width of 0.05.

The likelihood alone does not indicate whether the power law model is a good description of energy distribution. The average of the cumulative probability (§2.3) should be $\langle P(E_{\text{iso}}) \rangle = 1/2 \pm (12N)^{-1/2}$ for N bursts. Figure 6 shows that the cumulative $P(E_{\text{iso}})$ for $P_{\text{min}} = 0.5 \text{ ph cm}^{-2} \text{ s}^{-1}$ is very close to the straight line that is expected if the distribution function is a good description of the data. Although $\langle P(E_{\text{iso}}) \rangle = 0.4642 \pm 0.0089$ ($N = 1054$) formally differs by 4σ from the expected value of $1/2$, considering the likely systematic uncertainties (e.g., in the value of P_{min} , in the determination of the lags, in the corrections for the redshifting of high energy lightcurves), this value of $\langle P(E_{\text{iso}}) \rangle$ indicates that the distribution can be represented by a power law.

4.2.2. Lognormal E_{iso} Distribution

The second model distribution we consider is a lognormal energy distribution (see §2.5.1 of Band 2001); the parameters are the centroid $E_{\text{iso, cen}}$ and the logarithmic width σ_E of the distribution. For this distribution the posterior distribution (relevant to a Bayesian analysis) as a function of $\ln E_{\text{iso, cen}}$ and σ_E and the likelihood (relevant to a frequentist analysis) are the same if the prior is constant in $\ln E_{\text{iso, cen}}$ and σ_E . Figure 7 shows the likelihood surface; the peak occurs at $E_{\text{iso, cen}} = 3 \times 10^{51}$ ergs and $\sigma_E = 2.7$. However, as the figure shows, a broader distribution (larger σ_E) with a smaller centroid $E_{\text{iso, cen}}$ is not ruled out.

For $P_{\text{min}} = 0.5 \text{ ph cm}^{-2} \text{ s}^{-1}$ $\langle P(E_{\text{iso}}) \rangle = 0.4821 \pm 0.0089$ ($N = 1054$), which is consistent with $\langle P(E_{\text{iso}}) \rangle = 1/2$ at the 2σ level. Note that for $P_{\text{min}} = 0.3 \text{ ph cm}^{-2} \text{ s}^{-1}$ $\langle P(E_{\text{iso}}) \rangle = 0.4598 \pm 0.0085$ ($N = 1162$), which differs from the expected value by nearly 5σ . Figure 8 shows the distribution of the cumulative probability for $P_{\text{min}} = 0.5 \text{ ph cm}^{-2} \text{ s}^{-1}$; as can be seen, the observed cumulative probability distribution is consistent with the expected distribution.

5. Summary

We use the lag-luminosity relation to calculate self-consistently the redshifts for 1218 BATSE bursts. For the bursts without the spectral parameters required by the calculation we use average low and high energy spectral indices, and a peak energy E_p derived from the hardness ratio. We find that the redshift is quite sensitive to the spectral parameters. We use both single power law and broken power law lag-luminosity relations, and find that the broken power law relation does indeed predict a population of low luminosity, nearby bursts. For both forms of the relation the median redshift is 1.58.

We use the redshifts to calculate the apparent peak bolometric flux and the isotropic energy, both assuming that the bursts radiate isotropically.

We find that our burst data can be fit by a power law energy distribution with $\alpha = 1.76 \pm 0.05$ (95% confidence); considering only the statistical uncertainty the power law distribution is formally not a good fit, but with the likely systematic uncertainty the power law distribution is probably a good description of the data. While our power law fit is inconsistent with the original universal jet profile model (which predicts $\alpha = 2$), it is consistent with the jet profile models where parameters are permitted to vary.

A log-normal energy distribution also describes the data; the data permit a smaller average energy if the distribution is wider. More faint bursts will bound the lower end of this distribution.

REFERENCES

- Band, D. 2001, *ApJ*, 563, 582
- Band, D., et al. 1993, *ApJ*, 413, 281
- Bloom, J. S., Frail, D., & Kulkarni, S. 2003, *ApJ*, in press
- Fenimore, E. E., in't Zand, J. J. J. M., Norris, J. P., Bonnell, J. T., & Nemiroff, R. J. 1995, *ApJ*, 448, L101
- Fenimore, E. E., & Ramirez-Ruiz, E. 2000, *ApJ*, submitted [astro-ph/0004176]
- Frail, D., et al. 2001, *ApJ*, 562, 55
- Lloyd-Ronning, N., Dai, X., & Zhang, B. 2003, *ApJ*, submitted [astro-ph/0310431]
- Mallozzi, R., et al. 1998, in *Gamma-Ray Bursts, 4th Huntsville Symposium, AIP Conference Proceedings 428*, eds. C. Meegan, R. Preece and T. Koshut (AIP: Woodbury, NY), 273
- Norris, J. P. 2002, *ApJ*, 579, 386
- Norris, J. P., Marani, G. F., & Bonnell, J. T. 2000, *ApJ*, 534, 248
- Preece, R. D., Briggs, M. S., Mallozzi, R. S., Pendleton, G. N., Paciasas, W. S., & Band, D. L. 2000, *ApJS*, 126, 19
- Reichart, D. E., Lamb, D. Q., Fenimore, E. E., Ramirez-Ruiz, E., Cline, T. L., & Hurley, K. 2001, *ApJ*, 552, 57
- Rossi, E., Lazzati, D., & Rees, M. J. 2002, *MNRAS*, 332, 945
- Salmonson, J. 2001, *ApJ*, 546, 29
- Zhang, B., & Meszaros, P. 2002, *ApJ*, 571, 876
- Zhang, W., Woosley, S. E., & MacFayden, A. I. 2003, *ApJ*, 586, 356

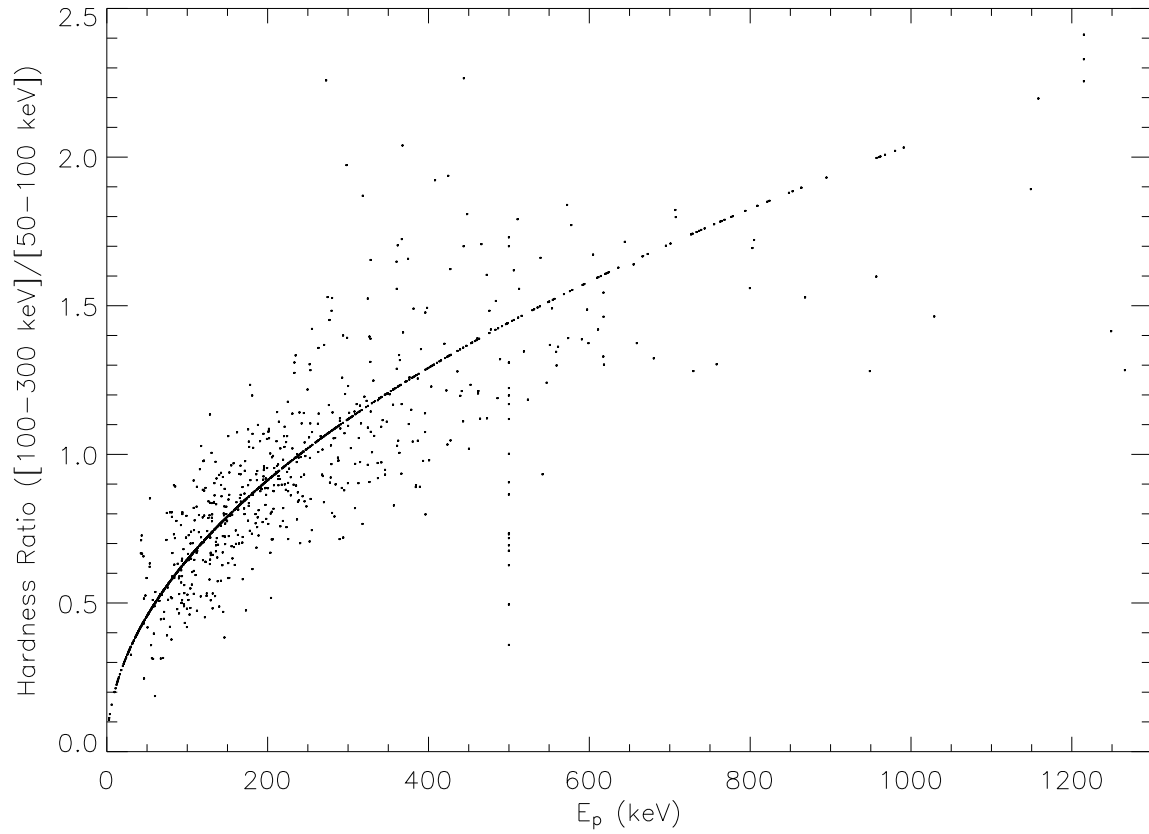


Fig. 1.— Hardness ratio HR_{32} (100–300 keV vs. 50–100 keV) as a function of E_p . Two populations are evident. First, spectral fits were not available for the bursts that fall on an empirical $E_p \propto \text{HR}_{32}^2$ relation. Second, bursts with spectral fits are dispersed around this $E_p \propto \text{HR}_{32}^2$ relation.

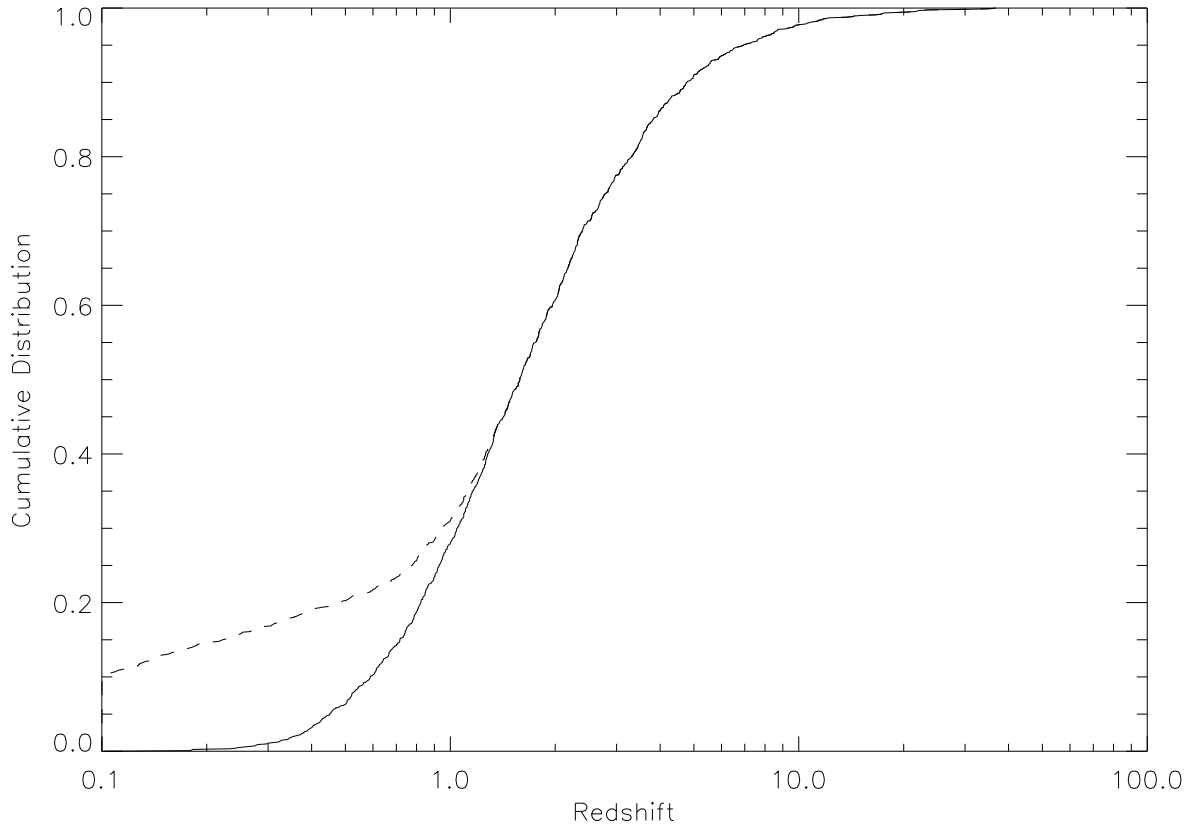


Fig. 2.— Cumulative distribution of bursts by redshift. Solid line—one component lag-luminosity relation. Dashed line—two component relation. Both distributions have the same median redshift of 1.6.

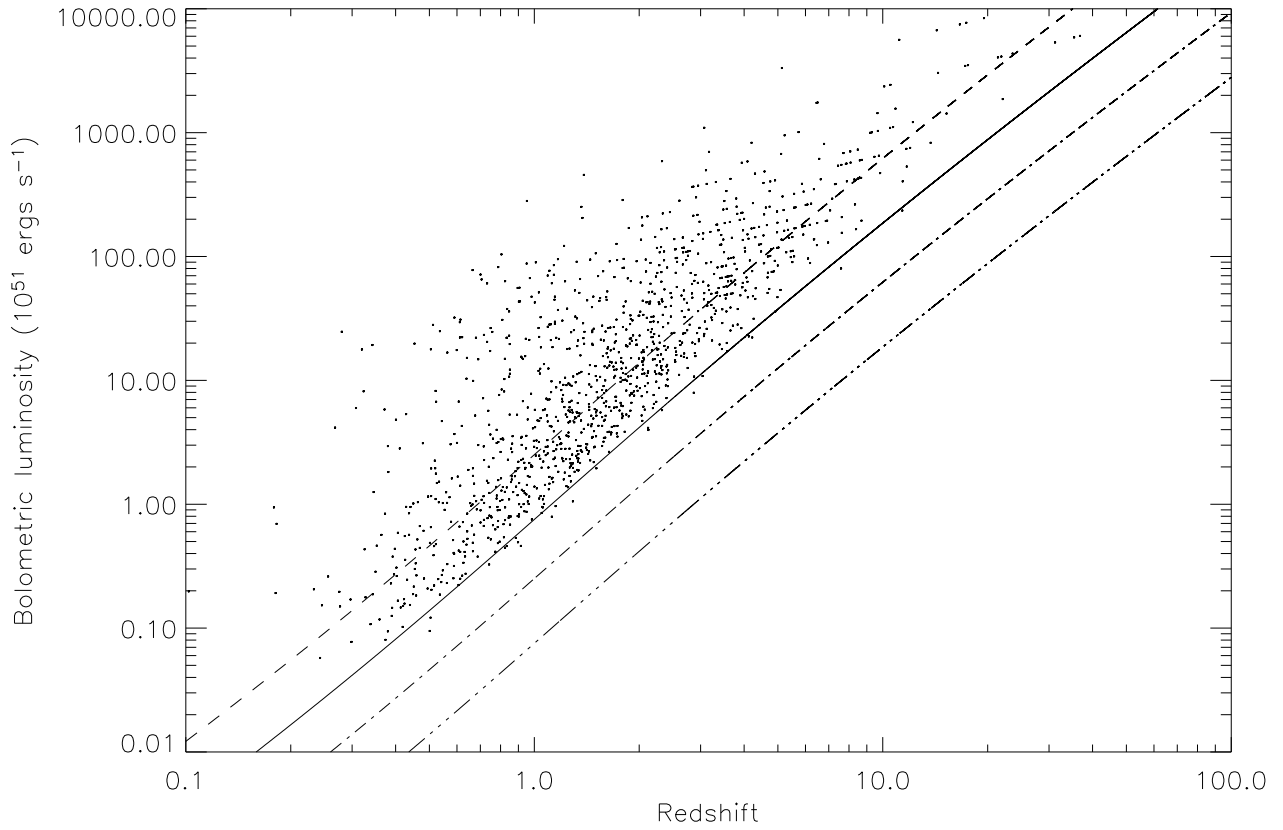


Fig. 3.— Bolometric peak luminosity L_B vs. redshift z for single component lag-luminosity relation. The lines represent the threshold peak luminosity for a threshold peak flux of $P > 0.3 \text{ ph cm}^{-2} \text{ s}^{-1}$ and $E_p = 30$ (2 dots-dashed line), 100 (dot-dashed), 300 (solid) and 1000 keV (dashed).

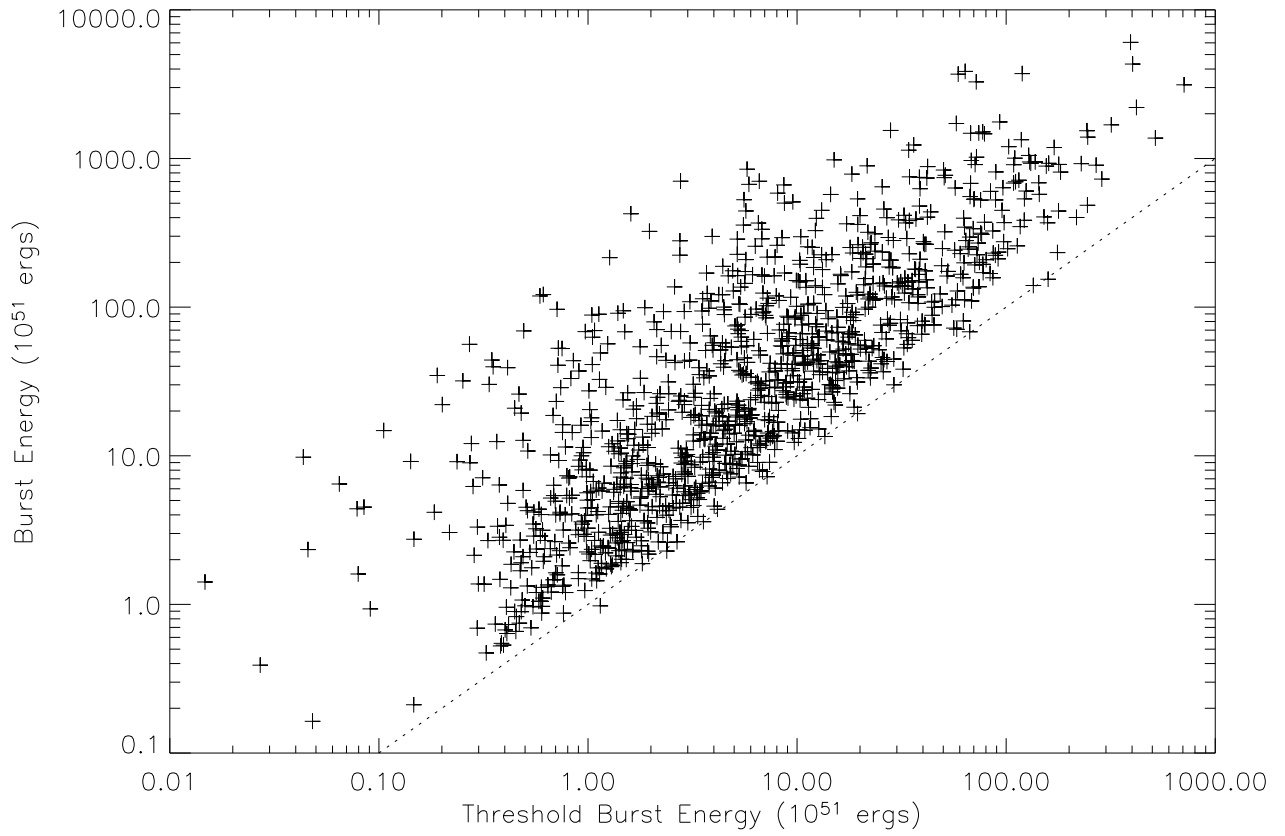


Fig. 4.— Scatter plot of E_{iso} vs. the $E_{\text{iso,min}}$. On the dotted line $E_{\text{iso}} = E_{\text{iso,min}}$. The paucity of bursts just above the dotted line suggests that P_{min} should be raised from 0.3 to $0.5 \text{ ph cm}^{-2} \text{ s}^{-1}$.

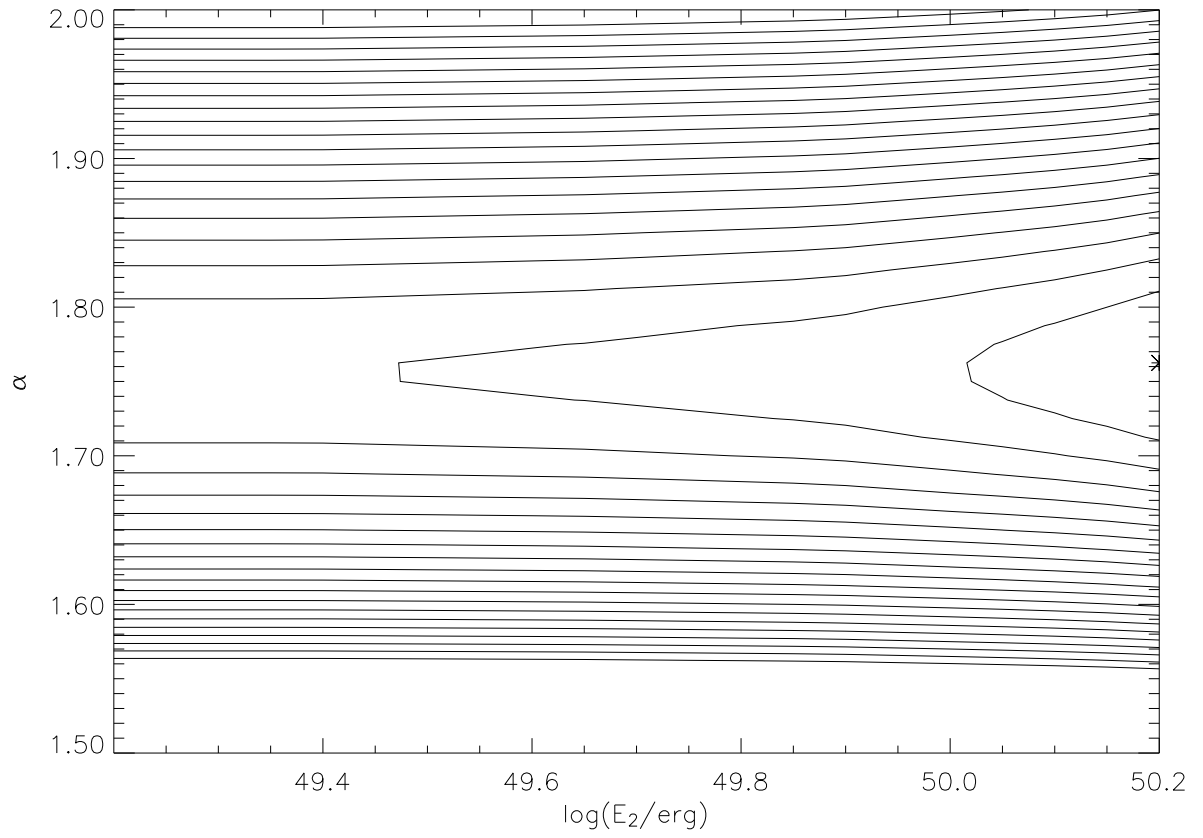


Fig. 5.— Contour plot of the likelihood function for a power law energy distribution. A threshold peak flux of $P_{\text{min}} = 0.5 \text{ ph cm}^{-2} \text{ s}^{-1}$ was imposed. The power law has an index of α and a low energy cutoff of E_2 .

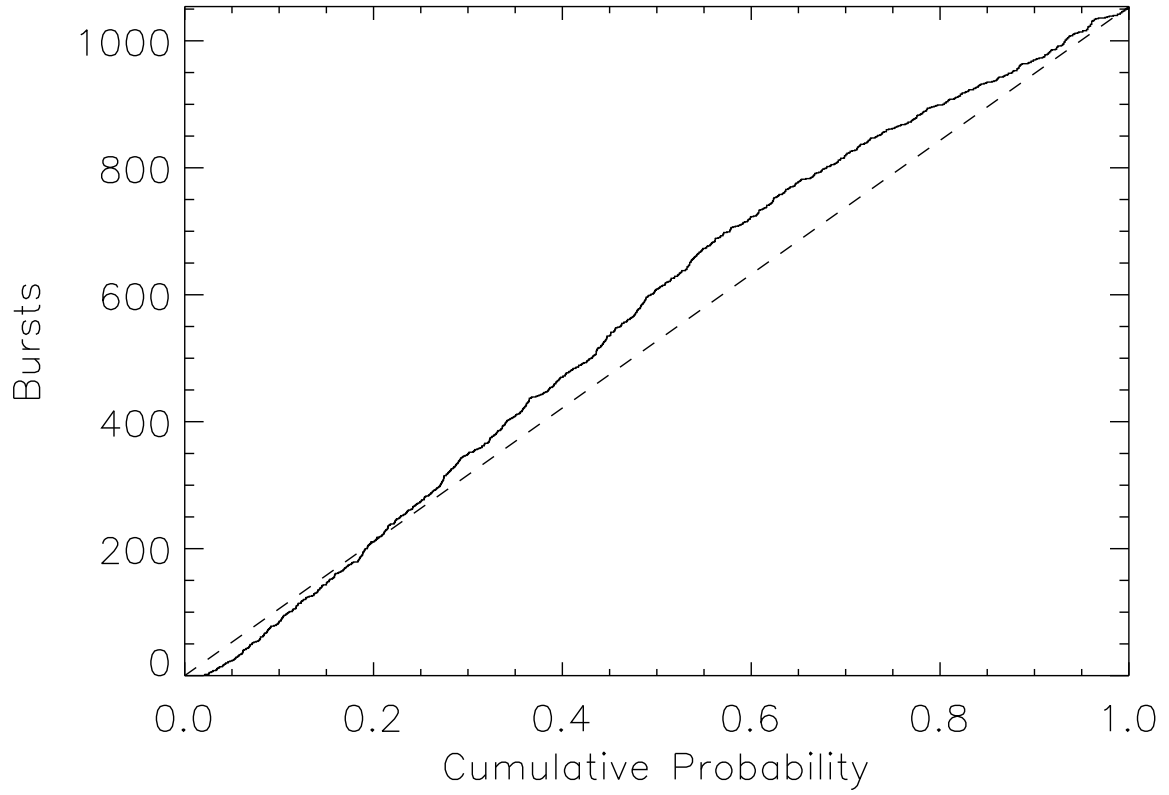


Fig. 6.— Cumulative distribution of the probability of the observed isotropic energies for a power law energy distribution. A threshold peak flux of $P_{\min} = 0.5 \text{ ph cm}^{-2} \text{ s}^{-1}$ was imposed.

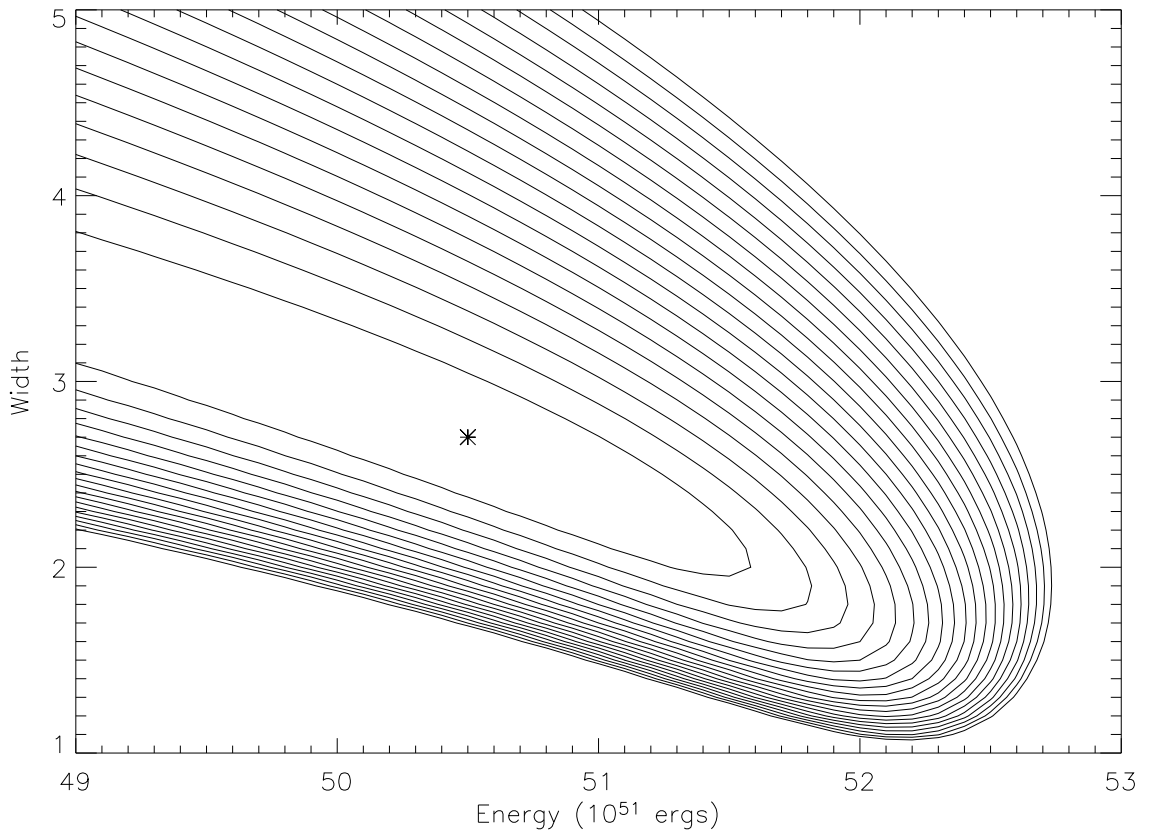


Fig. 7.— Contour plot of the likelihood function for a lognormal energy distribution. A threshold peak flux of $P_{\min} = 0.5 \text{ ph cm}^{-2} \text{ s}^{-1}$ was imposed. The distribution is characterized by a centroid energy and a logarithmic width.

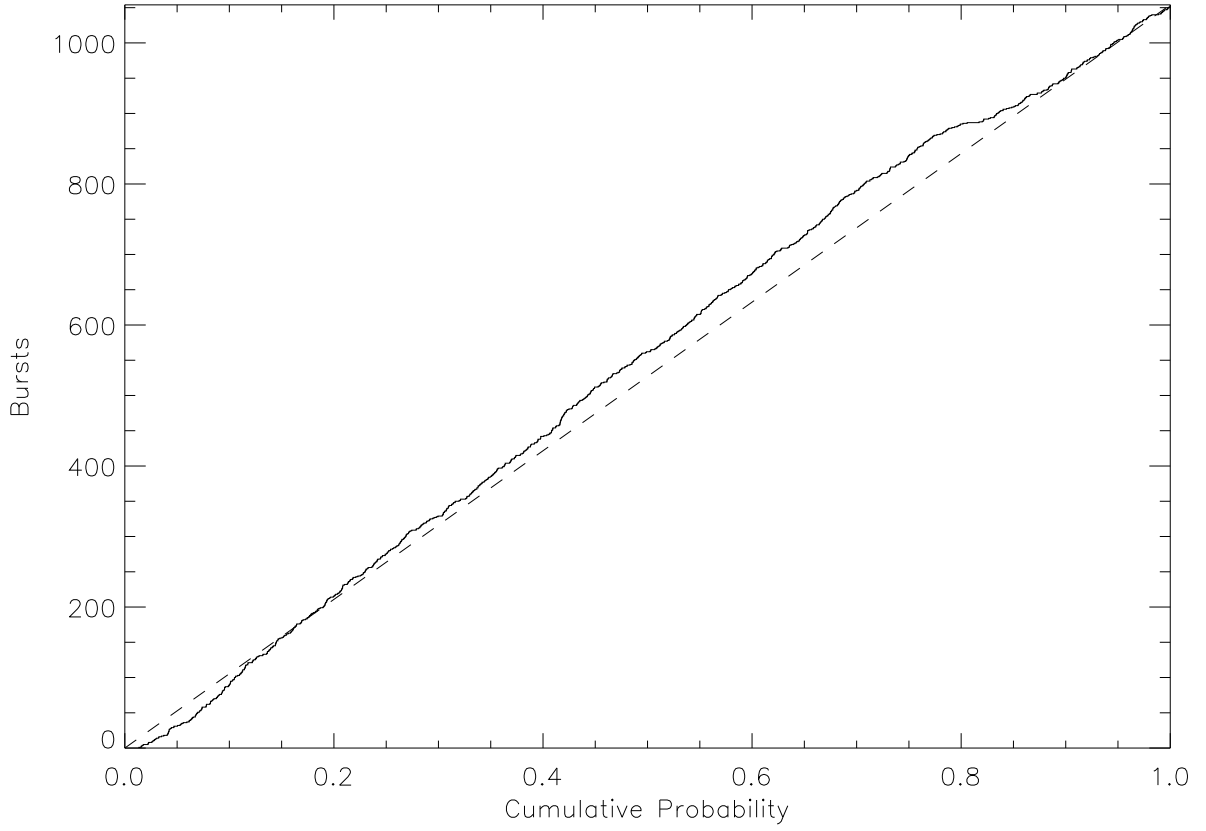


Fig. 8.— Cumulative distribution of the probability of the observed isotropic energies for a lognormal energy distribution. A threshold peak flux of $P_{\min} = 0.5 \text{ ph cm}^{-2} \text{ s}^{-1}$ was imposed.